View metadata, citation and similar papers at core.ac.uk

brought to you by CORE

provided by VU Research Portal

VU UNIVERSITEIT AMSTERDAM

VU Research Portal

Rotational dynamics of colloidal tracer spheres in suspensions of charged rigid rods

Koenderink, G.H.; Aarts, Dgal; Philipse, A. P.

published in
Journal of Chemical Physics
2003

DOI (link to publisher)
10.1063/1.1594182

document version
Publisher's PDF, also known as Version of record

Link to publication in VU Research Portal

citation for published version (APA)
Koenderink, G. H., Aarts, D., & Philipse, A. P. (2003). Rotational dynamics of colloidal tracer spheres in suspensions of charged rigid rods. *Journal of Chemical Physics*, *119*(8), 4490-4499. https://doi.org/10.1063/1.1594182

General rights
Copyright and moral rights for the publications made accessible in the public portal are retained by the authors and/or other copyright owners and it is a condition of accessing publications that users recognise and abide by the legal requirements associated with these rights.

- Users may download and print one copy of any publication from the public portal for the purpose of private study or research.
- You may not further distribute the material or use it for any profit-making activity or commercial gain
- You may freely distribute the URL identifying the publication in the public portal ?

Take down policy
If you believe that this document breaches copyright please contact us providing details, and we will remove access to the work immediately and investigate your claim.

E-mail address:
vuresearchportal.ub@vu.nl

Download date: 14. Sep. 2021

Rotational dynamics of colloidal tracer spheres in suspensions of charged rigid rods

Gijsberta H. Koenderink, Dirk G. A. L. Aarts, and Albert P. Philipse[a)]
Van't Hoff Laboratory for Physical and Colloid Chemistry, Debye Institute, Utrecht University, Padualaan 8, 3584 CH Utrecht, the Netherlands

(Received 2 May 2003; accepted 2 June 2003)

The short-time rotational dynamics of colloidal silica tracer spheres in suspensions of rigid silica rods is investigated, using time-resolved phosphorescence anisotropy, as a function of tracer radius a_T, rod volume fraction ϕ, and the range κ^{-1} of the double-layer repulsions between the like-charged rods and tracer spheres. A large tracer size a_T and a small screening length κ^{-1} appear to maximize hydrodynamic hindrance of tracer diffusion for given ϕ. The marked ϕ-dependence of the rotational dynamics is primarily determined by the large excluded volumes of the high-aspect ratio rods. Stokes–Einstein–Debye (SED) scaling of the rotational diffusion coefficients with the inverse viscosity of the rod suspensions holds fairly well, expect for small a_T and large κ^{-1}. The ionic strength dependence of deviations from SED scaling is rationalized in terms of an effective hard-rod model with the bare length L replaced by an effective length $L+4\kappa^{-1}$. © *2003 American Institute of Physics.* [DOI: 10.1063/1.1594182]

I. INTRODUCTION

The structural and dynamical properties of a colloidal suspension strongly depend on the shape of its constituents. Suspensions of rod- or platelike particles, for instance, have very different macroscopic properties compared to suspensions of spherical particles, owing to the large excluded volume of a strongly anisometric particle relative to its volume. An example of such a shape effect is the formation of space-filling gels of randomly oriented rodlike particles at very low solid contents.[1] This space-filling efficiency is exploited by biological cells, which possess a tough elastic framework of rodlike macromolecules, called the cytoskeleton, which provides structural stability while also providing sufficient porosity to allow transport of proteins and organelles within the cell cytoplasm. Another striking shape anisotropy effect is the large viscosity of rod[2] and plate[3] suspensions at very low volume fractions, which makes anisometric particles and macromolecules widely applied additives to control the flow properties of industrial and commercial particle suspensions. Rodlike particles are also known to very effectively retard particle transport. Both theoretical[4–7] and experimental[8–12] work has been done on the translational diffusion of spherical tracer particles in host suspensions of rods, showing that host rods retard tracer diffusion at much lower volume fractions than host spheres. Rotational diffusion of tracer spheres in rod suspensions has, to our knowledge, not been studied yet.

In this paper we present the first measurements of the rotational dynamics of tracer spheres in isotropic suspensions of charged rigid rods. This extends our previous experimental studies of rotational diffusion in charge-stabilized binary sphere mixtures.[13–16] Our colloidal model system comprises phosphorescently labeled silica tracer spheres dispersed in nonaqueous suspensions of like-charged silica-coated host rods. The range of the electrostatic double-layer repulsions is varied by changing the ionic strength. The rotational diffusion coefficients of the tracer spheres are measured with time-resolved phosphorescence anisotropy (TPA). This technique employs a linearly polarized light pulse to create an orientationally anisotropic subset of excited-state fluorophores inside the tracer colloids, with absorption dipole moments along the polarization direction. The rotational diffusion coefficient is extracted from the gradual depolarization of the phosphorescence emitted from the excited state decay. An advantage of TPA compared to other techniques like depolarized dynamic light scattering[13,17] (DDLS) and nuclear magnetic resonance[18] (NMR) is that the required tracer particles are relatively easy to synthesize. Phosphorescent labeling is straightforward[19] and can be applied to a variety of tracer colloids, which can be surface-functionalized to control the particle interactions.[15] In contrast, DDLS and NMR require special tracer colloids that are difficult to synthesize, being either optically anisotropic or labeled with isotopes such as ^{2}H or ^{13}C.

In this paper we focus on three issues. First, we compare the data with experimental and theoretical results for tracers in sphere suspensions, to elucidate the effect of the host particle shape. Second, we explore the ionic strength dependence of the rotational tracer dynamics. Previously[13–16] we showed that rotational diffusion of tracer spheres in sphere suspensions is highly sensitive to the local microstructure and to the interaction potential near contact. Finally, we compare the rotational dynamics with the bulk rheology of the host suspensions, motivated by the familiar Stokes–Einstein–Debye (SED) relation for a colloidal sphere in solvent[16]

[a)]Author to whom correspondence should be addressed. Electronic mail: fccoffice@chem.uu.nl

 © 2003 American Institute of Physics

Downloaded 30 Mar 2011 to 130.37.129.78. Redistribution subject to AIP license or copyright; see http://jcp.aip.org/about/rights_and_permissions

TABLE I. Relative size polydispersity σ_{TEM}, hydrodynamic particle radii a_{DLS} and a_{TPA}, initial phosphorescence anisotropy r_0, and rotational decay time τ_{rot} of silica tracer spheres.

Particle	σ_{TEM}[a]	a_{DLS} [nm][b]	a_{TPA} [nm][c]	r_0[c]	τ_{rot} [ms][c]
μ10	1.5%	72	67	0.108	0.39
μ30	2.7%	100	103	0.110	1.44
P113	10%	124	137	0.121	3.00

[a]Determined by image analysis of TEM micrographs.
[b]From the translational diffusion coefficient $D_0^t = k_B T/(6\pi\eta_0 a_T)$, measured with dynamic light scattering.
[c]Measured with TPA.

$$D_0^r = \frac{k_B T}{8\pi\eta_0 a_T^3}. \tag{1}$$

Here, η_0 is the solvent viscosity, and $k_B T$ is the thermal energy.

When a tracer is immersed in a colloidal suspension of rods instead of a simple solvent, its rotational dynamics will be reduced by hydrodynamic and direct interactions with the rods. The question is whether this reduction can be captured by a generalized version of Eq. (1) with η_0 replaced by the concentration dependent viscosity of the rod suspension. Such a generalization clearly is an approximation, since the rods have comparable characteristic length and diffusion time scales as the tracer sphere. Furthermore, rotational diffusion of tracer spheres in a colloidal host suspension is frequency dependent due to colloidal interactions. At infinite frequencies (''short times'') the host particle configuration is essentially static in the time $\tau_{2\pi} = 1/D_0^r$ it takes the tracer sphere to diffuse 2π radians, so the tracer dynamics is affected only by hydrodynamic interaction. The tracer dynamics is diffusive and characterized by a short-time diffusion coefficient, D_s^r. At finite frequencies the host particle configuration is evolving and the tracer dynamics is generally nondiffusive, except in the limit of zero frequency (''long times''). In this limit the host suspension microstructure has relaxed and the tracer has experienced many statistically independent rod configurations during a time $\tau_{2\pi}$. Its diffusion coefficient, D_L^r, is thus affected both by hydrodynamic interactions and by direct particle interactions (memory effects). The separation of time scales in a concentrated host suspension suggests the following heuristic generalization of the SED relation

$$D_s^r = \frac{k_B T}{8\pi\eta_\infty a_T^3} (\text{short times}), \tag{2a}$$

$$D_L^r = \frac{k_B T}{8\pi\eta_L a_T^3} (\text{long times}), \tag{2b}$$

involving the infinite frequency viscosity η_∞, a purely hydrodynamic quantity, and the low-shear-limiting viscosity η_L, which like D_L^r reflects a combination of hydrodynamic and direct interactions. The rotational diffusion coefficients reported here are short-time quantities, affected only by hydrodynamic interactions. The structural relaxation time τ_I of the rod suspensions is at least 10 ms, taking for τ_I the time required for a rod to diffuse over its length L, while the characteristic rotation time $\tau_{2\pi}$ of the tracer spheres is about 1 ms. (L is 203 nm on average, and the translational diffusion coefficient of a rod is 4×10^{-12} m^2/s at infinite dilution.) The data should therefore be compared to experimental data and/or theoretical predictions for the infinite-frequency viscosity η_∞ of the rod suspensions, according to Eq. (2a). Measurements of η_∞ were, however, prevented by the large sample volumes ($\geqslant$20 mL) required, while theoretical calculations[20] of η_∞ are so far limited to rods of infinite aspect ratio. Instead, we therefore compare the measured diffusion coefficients with the experimentally determined low-shear-limiting viscosity η_L of the rod suspensions. We discuss how the continuum assumption underlying the generalized SED relations is affected by the tracer–host size ratio, the host particle concentration, and the range of electrostatic double layer interactions.

II. EXPERIMENT

A. The colloidal model system

Tracer particles were colloidal silica spheres, covalently labeled with the phosphorescent dye eosin-5-isothiocyanate. Three sets of particles were used, coded μ10, μ30, and P113. Particles μ10 ($a_T = 67$ nm) and μ30 ($a_T = 103$ nm) have a nonphosphorescent core (22 nm radius), obtained with a micro-emulsion synthesis, covered with an eosin-labeled silica shell.[15] Particles P113 ($a_T = 137$ nm) were prepared by a Stöber synthesis and contain an eosin-labeled core.[19] Table I lists relevant characteristics of the particles. The tracers acquire a negative surface charge in N,N-dimethylformamide (DMF) due to dissociation of the acid silanol groups on their surfaces. The zeta potential in DMF containing LiCl is of order -30 mV.

The colloidal host rods, coded B1S3, were prepared by coating boehmite (γ-AlOOH) cores[21] having an average length of 194 nm and diameter of 9 nm with a 4.5 nm thick silica shell according to the procedure of van Bruggen *et al.*[22] Figures 1(a) and 1(b) show typical transmission electron microscopy (TEM) images of the rods. The number averaged length $\overline{L}$ and diameter $\overline{D}$ of the rods determined from TEM are 203 ± 93 nm and 18 ± 3 nm, respectively [Figs. 1(c) and 1(d)]. The translational diffusion coefficient at infinite dilution, determined by dynamic light scattering (DLS), is 4.03×10^{-12} m^2/s, which is a factor two smaller than theoretically predicted for smooth hard rods.[23] This discrepancy conforms to earlier diffusion results for silica-boehmite rods in DMF.[12,24] The deviation is likely due to the surface roughness of the rods, visible in Fig. 1(b). The rods are negatively charged in DMF due to dissociation of the surface silanol

Downloaded 30 Mar 2011 to 130.37.129.78. Redistribution subject to AIP license or copyright; see http://jcp.aip.org/about/rights_and_permissions

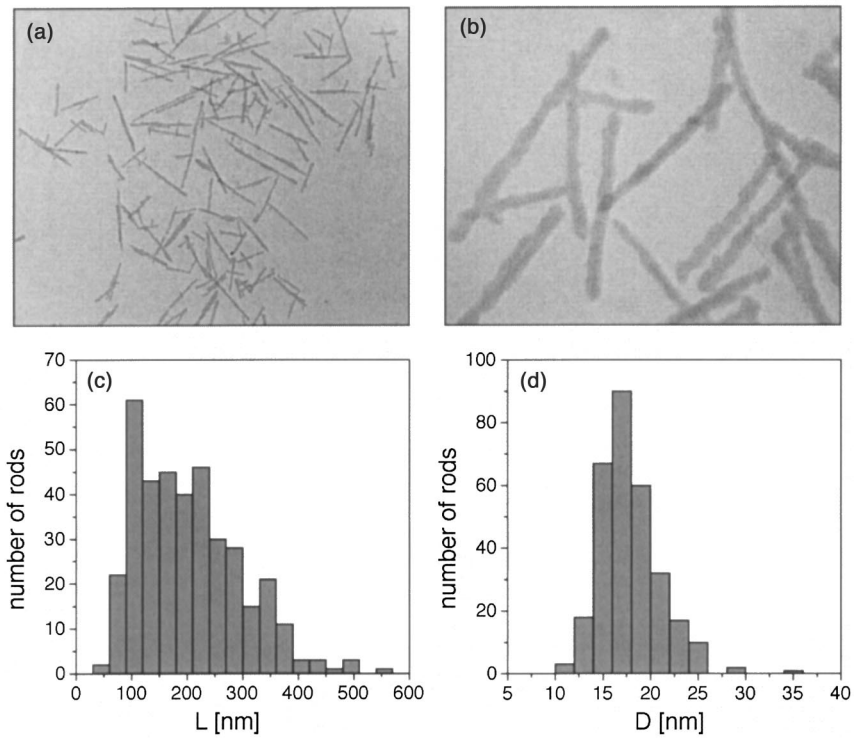

FIG. 1. (a) and (b) Transmission electron microscopy (TEM) images of the silica-boehmite rods. (c) Image analysis results for the rod lengths L (total number 375), with average length $\overline{L}=203$ nm and relative standard deviation of 46%. (d) Image analysis results for the rod diameters D (total number 300), with average diameter $\overline{D}=18$ nm and relative standard deviation of 18%.

groups in DMF. At a LiCl concentration of 10 mM, the zeta potential is -24 mV, as determined from mobility measurements with a Coulter DELSA 440 SX instrument. Mass fractions were converted to volume fractions ϕ using a particle mass density of 2 g/mL, which is a volume average of the densities of silica and boehmite.

The solvent DMF has a refractive index n_s of 1.430 and dielectric constant ε of 38 at 20 °C. The refractive index of DMF is close to that of the silica tracer spheres and of the silica shell of the rods ($\approx$1.45), minimizing rod–rod and rod–sphere van der Waals attractions.[22] The rod suspensions remained stable up to LiCl concentrations of at least 0.25 M. This exceptional stability is probably in part due to strong solvation of silica surfaces in DMF, which leads to a strong repulsion with a range of 3–5 nm.[15,25,26] The range of the double-layer repulsions between the particles is controlled by the Debye screening length κ^{-1}, which is in turn determined by the number density n_s of electrolyte (assumed univalent)

$$\kappa^{-1}=\sqrt{\frac{\varepsilon_0\varepsilon k_B T}{2e^2 n_s}}, \tag{3}$$

where e is the elementary charge and ε_0 the vacuum permittivity. The rod–sphere mixtures contained 0, 10, or 100 mM LiCl. LiCl concentrations of 10 and 100 mM correspond to screening lengths κ^{-1} of 2.3 and 0.95 nm. The salt-free rod suspensions contain a significant background electrolyte concentration due to dissociated counterions from the rods. (Autodissociation of DMF is negligible, the ionization constant pK_{auto} being about 29.[27]) Total internal reflection microscopy (TIRM) measurements of the interaction potential of a polystyrene sphere with a flat silica wall indicate a screening length of about 50 nm in pure DMF, i.e., 0.02 mM (univalent) electrolyte.[26,28] At a rod volume fraction $\phi=0.002$ a total (univalent) electrolyte concentration of close to 0.1 mM was estimated from TIRM measurements, corresponding to $\kappa^{-1}(\phi)=21$ nm.[28]

B. TPA measurements of rotational diffusion

Rotational diffusion coefficients of dilute tracer spheres (volume fraction <0.005) in rod suspensions were measured with time-resolved phosphorescence anisotropy (TPA). A brief summary of the measurement principle[15,19,29] is presented here. The sample is exposed to a short (5 ns) pulse of linearly polarized light, which excites the phosphorescent dye molecules from the singlet ground-state S_0 to the first excited singlet state S_1. The probability P_A for absorption of a photon with polarization $\hat{A}$ depends on the orientation of the absorption dipole moment $\hat{\mu}_a$ of the dye molecule with respect to $\hat{A}$

$$P_A \propto |\hat{\mu}_a \cdot \hat{A}|^2, \tag{4}$$

so a polarized light pulse produces an orientationally anisotropic subset of excited fluorophores. Some of these excited molecules revert to the triplet excited-state T_1 via intersystem crossing. Phosphorescence occurs when molecules in the T_1 state relax to the S_0 state by emitting a photon. The phosphorescence intensity is measured through an emission polarizer with a direction $\hat{E}$. The probability for emission of a photon with a direction $\hat{E}$ depends on the direction of the emission dipole moment $\hat{\mu}_e$ with respect to $\hat{E}$

$$P_E \propto |\hat{\mu}_e \cdot \hat{E}|^2. \tag{5}$$

Downloaded 30 Mar 2011 to 130.37.129.78. Redistribution subject to AIP license or copyright; see http://jcp.aip.org/about/rights_and_permissions

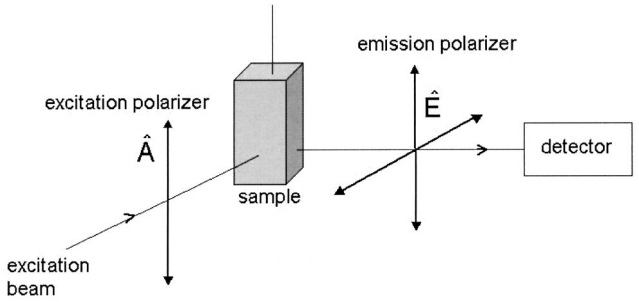

FIG. 2. Schematic depiction of the TPA experiment. The polarization directions of the incident and emitted light are defined with a polarizer ($\hat{A}$) and analyzer ($\hat{E}$), respectively. The polarization $\hat{A}$ is always vertical, while $\hat{E}$ is switched between the vertical and horizontal direction.

The time-dependent phosphorescence intensity $I(t)$ is an ensemble average of $P_A(0)P_E(t)$ over all possible orientations of the dye molecules in the illuminated volume, assuming an infinitesimally short excitation pulse:

$$I(t)=C_{\exp}F(t)\langle|\hat{A}\cdot\hat{\mu}_A(0)|^2|\hat{E}\cdot\hat{\mu}_E(t)|^2\rangle. \tag{6}$$

The prefactor $C_{\exp}$ accounts for the dye concentration, phosphorescence quantum yield and detector efficiency. The isotropic function $F(t)$ gives the probability that a molecule is still in the excited state at time t after the application of an excitation pulse at $t=0$. Since the $T_1\rightarrow S_0$ transition is spin-forbidden, the phosphorescence lifetime is quite long, being of order milliseconds (3 ms in case of eosin).

In this work the conventional 90° arrangement for luminescence depolarization experiments sketched in Fig. 2 was used. The excitation beam polarization $\hat{A}$ is fixed along the vertical orientation. The phosphorescence is detected at right angles to the excitation beam, through a polarizing filter along $\hat{E}$ that is switched between an orientation parallel and perpendicular to $\hat{A}$. The corresponding phosphorescence intensities are denoted as $I_{\parallel}(t)$ and $I_{\perp}(t)$, respectively. The total intensity

$$\Delta I_{\text{tot}}(t)=I_{\parallel}(t)+2I_{\perp}(t)=\tfrac{1}{3}C_{\exp}F(t) \tag{7}$$

gradually decays to zero because the T_1 excited-state relaxes to the S_0 ground state, posing an upper limit to the experimentally accessible rotational correlation times ($\sim$10 ms in case of eosin). The dimensionless anisotropy

$$r(t)=\frac{I_{\parallel}(t)-I_{\perp}}{I_{\text{tot}}(t)}=\frac{2}{5}\langle P_2[\hat{\mu}_a(0)\cdot\hat{\mu}_e(t)]\rangle \tag{8}$$

decays due to orientational randomization of the excited-state molecules as the labeled colloidal particles perform rotational Brownian motion. In addition, there is generally some limited rotational mobility of the dye molecules inside the particles. The anisotropy gives the ensemble averaged correlation between the orientations of the absorption dipole moment $\hat{\mu}_a(0)$ at time zero, and the emission dipole moment $\hat{\mu}_e(t)$ at time t. $P_2(x)$, defined as $P_2=(3x^2-1)/2$, is the second-order Legendre polynomial. On the colloidal time scale (10^{-3} s) the fluorophores have already fully explored the space available to them inside the colloids at $t=0$, so the time-dependence of $r(t)$ is determined only by the dynamics of the colloids. In case of noninteracting, monodisperse colloidal tracer spheres the rotational dynamics is described by the Debye model,[30] so

$$r(t)=r_0\exp(-6D_0^r t), \tag{9}$$

where D_0^r is the rotational diffusion coefficient specified in Eq. (1). When the dye molecules are rigidly anchored, r_0 has a theoretical maximum of 0.4, when $\hat{\mu}_a$ and $\hat{\mu}_e$ are co-linear. The maximum zero-time anisotropy for eosin is only 0.19, because $\hat{\mu}_e$ makes an angle of 36° with $\hat{\mu}_a$.[31] Rotational mobility of the dye molecules inside the colloidal particles also lowers the initial anisotropy. In practice, r_0 is often further decreased due to energy transfer between the dye molecules. For the eosin-labeled silica tracer spheres used here, r_0 is typically about 0.1 (cf. Table I). When the tracer spheres are dispersed in concentrated suspensions of host particles, the anisotropy decay may become nonexponential due to direct particle interactions. The anisotropy decay curves in this study, however, were single-exponential for all rod volume fractions studied, with a decay time $1/(6D_s^r)$, where D_s^r is the short-time rotational tracer diffusion coefficient.

The TPA measurements were performed in a temperature-controlled room (23 °C), using the same setup used earlier to measure rotational diffusion in binary sphere suspensions.[14,15] The eosin dye was excited by short (5 ns) pulses from a Nd:yttrium-aluminum-garnet (YAG) laser with a wavelength of 532 nm. The samples were contained in narrow glass capillaries (VitroDynamics) immersed in toluene, to optically match the glass, and kept at an angle of 45° with the excitation beam. The phosphorescent light was measured with a photomultiplier, after passing through an interference filter that discards scattered excitation light, and a sheet polarizer mounted on a rotation stage. Measurements consisted of several sequences of alternately measuring $I_{\parallel}(t)$ and $I_{\perp}(t)$. The phosphorescence intensities were corrected for the different transmission efficiency of the detection line for vertically and horizontally polarized light. The correction factor, $G=I_{\text{HH}}/I_{\text{HV}}=0.86$, was obtained by measuring the intensities I_{HH} and I_{HV} upon excitation with horizontally polarized light.

C. Viscosity measurements on host rod suspensions

Low-shear-limiting viscosities η_{L} of the host rod suspensions were measured at 25 °C using a strain-controlled Contraves low shear rheometer with Couette geometry (gap width 0.504 mm), applying a simple steady shear with shear rates $\dot{\gamma}=0-50\ \text{s}^{-1}$. The viscosities were normalized by the solvent viscosity, η_0 (0.795 mPa.s for pure DMF).

III. RESULTS AND DISCUSSION

A. Ionic strength dependence of rotational tracer dynamics in rod suspensions

Figures 3(a)–3(c) present the reduced short-time rotational diffusion coefficients $H_s^r(\phi)=D_s^r(\phi)/D_0^r$ of tracer spheres with radii a_T of 67, 103, and 137 nm, respectively, as a function of the rod volume fraction ϕ. At all LiCl concentrations studied (0, 10, and 100 mM), raising the rod concentration leads to a monotonic reduction of the tracer mobility.

Downloaded 30 Mar 2011 to 130.37.129.78. Redistribution subject to AIP license or copyright; see http://jcp.aip.org/about/rights_and_permissions

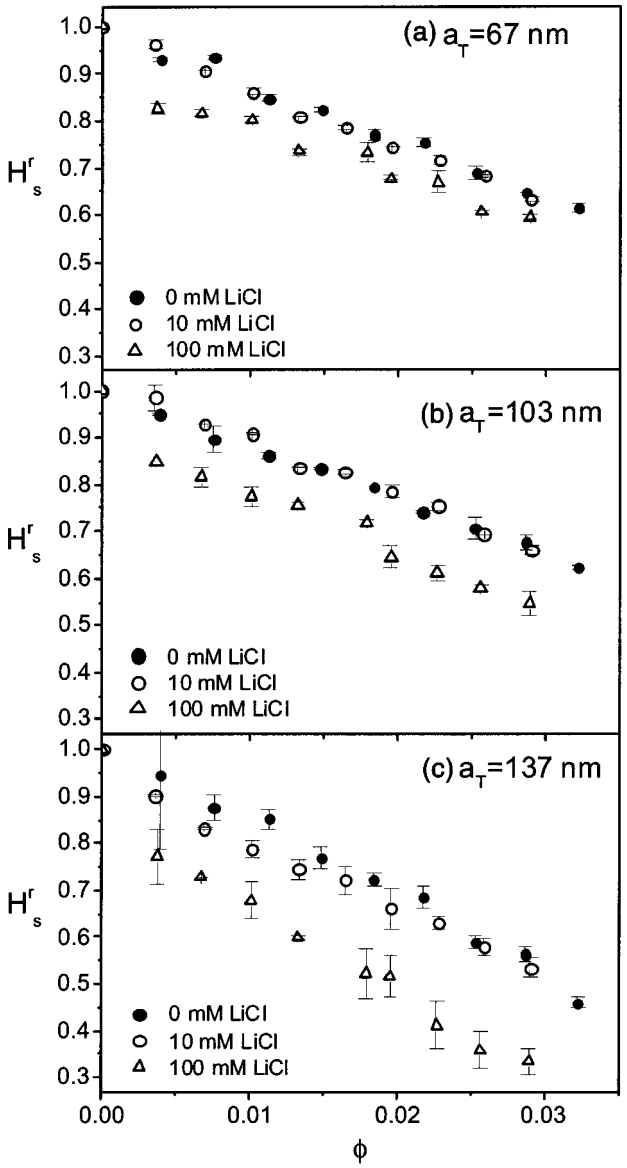

FIG. 3. Reduced short-time rotational diffusion coefficient H_s^r of charged tracer spheres in host suspensions of charged rods dispersed in DMF, with LiCl concentrations as indicated. The tracer sphere radius a_T is (a) 67 nm, (b) 103 nm, and (c) 137 nm.

All three tracers qualitatively display the same dependence of H_s^r on the ionic strength, which can be summarized as $H_s^r(0\ \mathrm{mM}) \approx H_s^r(10\ \mathrm{mM}) > H_s^r(100\ \mathrm{mM})$. The fact that $H_s^r(0\ \mathrm{mM})$ is almost identical to $H_s^r(10\ \mathrm{mM})$ is surprising, since adding 10 mM LiCl reduces the Debye screening length κ^{-1} from ~20 to 2 nm. One would expect increased screening of double layer repulsions to reduce H_s^r: addition of salt brings the particles closer together, leading to stronger hydrodynamic hindrance of rotational tracer diffusion. Though calculations of the hydrodynamic hindrance experienced by a rotating tracer sphere in a dilute suspension of rods are unavailable to confirm our expectation, we anticipate qualitatively similar behavior as in dilute host sphere suspensions.

Calculations of the ionic strength dependence of H_s^r for tracer rotation in sphere suspensions were reported by Nägele and co-workers.[14,32] For dilute suspensions of host spheres, H_s^r can be expanded in powers of ϕ according to $H_s^r = 1 - H_{s1}^r(\phi,\lambda)\phi + \mathrm{O}(\phi^2)$, where $\lambda = a_T/a_H$ is the tracer–host sphere size ratio. The coefficient H_{s1}^r represents the equilibrium ensemble-averaged effect on rotational diffusion of pair hydrodynamic interactions between one tracer sphere with radius a_T and one host particle with radius a_H

$$H_{s1}^r(\phi,\lambda) = \int_{a_T+a_H}^{\infty} g_{TH}^{(2)}(r;\lambda,\phi) A_{TH}^{rr}(r;\lambda) r^2 dr. \qquad (10)$$

This integral involves the radial distribution function $g_{TH}^{(2)}(r;\phi,\lambda)$, giving the conditional probability of finding a host sphere a center-to-center distance r away from a tracer sphere. The hydrodynamic mobility function $A_{TH}^{rr}(r;\lambda)$ accounts for pair hydrodynamic interactions and can be expressed as a multipole expansion in even powers of r^{-1}. $A_{TH}^{rr}(r;\lambda)$ is fairly short-ranged, with a leading term proportional to r^{-6}. Accordingly, the main contribution to the integral in Eq. (10) originates from particle configurations near contact. At low ionic strengths the average tracer–host distance is large owing to the long-ranged double layer repulsions, so the rotational dynamics of a tracer is only weakly hindered. At high ionic strengths, on the other hand, the pair correlation function has its principal peak near particle contact ($r = a_T + a_H$), and hydrodynamic hindrance is enhanced. We do not expect the orientation dependence of hydrodynamic interactions in a rod–sphere mixture to qualitatively change this behavior. We therefore anticipated a decrease of H_s^r on addition of 10 mM LiCl and a negligible change upon further addition of 100 mM LiCl. The experimental observations are at variance with these expectations, but in line with TPA results for mixtures of tracer and host spheres in a solvent mixture of DMF and dimethylsulfoxide (DMSO) with $a_T/a_H = 1$.[15] In the latter case, rotational diffusion data for 0 M LiCl and 10 mM LiCl coincided within experimental error, and rotational diffusion became slower only when 100 mM LiCl was added. For the same tracers dispersed in suspensions of larger host spheres ($a_T/a_H = 0.32$), however, the TPA data did reveal an immediate reduction of H_s^r on addition of 10 mM LiCl to a salt-free suspension, in qualitative agreement with theory.

The surprising ionic strength dependencies observed for rod–sphere mixtures as well as binary sphere mixtures with $a_T/a_H = 1$ suggest that the available theoretical description is incomplete. One feature not present in the theory is the strong solvation of silica surfaces in DMF (and DMSO), mentioned in Sec. II B. Solvation contributes a short-range repulsion that becomes important when the double layers are largely screened. TIRM measurements of double layer interaction potentials between a silica surface and a large polystyrene sphere in DMF suggest that as soon as κ^{-1} is less than about 10 nm the solvation repulsion has a significant effect on the suspension microstructure.[26,28] Short-time rotational tracer diffusion is highly sensitive to the interactions of the tracer with host particles at separations close to contact due to the short range of the hydrodynamic interactions. It, therefore, seems likely that solvation effects have a significant impact on rotational diffusion. A second feature not incorporated in the theory for rotational diffusion is the nature of the charge regulation mechanism, which becomes impor-

Downloaded 30 Mar 2011 to 130.37.129.78. Redistribution subject to AIP license or copyright; see http://jcp.aip.org/about/rights_and_permissions

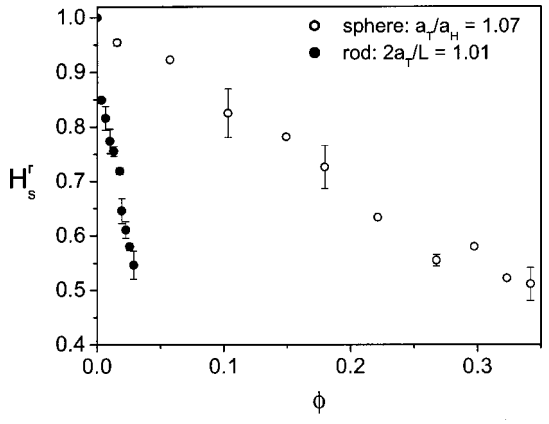

FIG. 4. Reduced short-time rotational diffusion coefficient $H_s^r(\phi)$ of charged $\mu 30$ tracer spheres ($a_T = 103$ nm) in suspensions of host spheres ($a_T = 96$ nm) and host rods ($\overline{L} = 203$ nm) in DMF with 100 mM LiCl added to screen electrostatic repulsions.

tant when the particles approach each other closely. Calculations for charged spheres so far always assumed a constant surface charge density, while in reality the charge density of silica surfaces is dependent on the interparticle distance and the ionic strength.[33] The experimental observations reported here certainly call for an extension of the theory to include charge regulation, i.e., a distance (and κ^{-1}) dependent charge density on the particles.

B. Tracer dynamics in rod and sphere suspensions: Shape effect

In this section we attempt a quantitative comparison of the data for host rods with experimental data for host spheres and we investigate whether simple geometrical arguments can account for the different effect of rod and sphere suspensions on the rotational dynamics of immersed tracer spheres.

Figure 4 compares rotational diffusion coefficients of $\mu 30$ tracers ($a_T = 103$ nm) in suspensions of host rods and suspensions of silica host spheres with a diameter $2a_H = 192$ nm, practically equal to the number average length $\overline{L}$ of the rods. The host spheres and rods have the same silica chemistry and are dissolved in very comparable electrolyte solutions, namely DMF for the rods and DMF-DMSO 3:7 v/v for the spheres, both containing LiCl. The data are compared in the high-salt limit (100 mM LiCl), so the Debye screening length is less than 1 nm in both cases and the electrostatics are largely screened.

It is immediately obvious that at the same filling fraction the rods much more drastically hinder tracer diffusion. The volume fraction of host rods needed to reduce H_s^r by a given amount is smaller than in the case of host spheres by a factor of 10, which is close to the rod aspect ratio L/D. In fact, multiplying the rod volume fraction ϕ with L/D fairly accurately rescales the rod data on top of the sphere data, as shown in Fig. 5(a). This suggests that the shape effect can be understood in terms of the different excluded volumes of rods and spheres.

The orientationally averaged volume that one rod excludes to a second rod, in the limit of vanishing rod thickness, is given by the well-known Onsager result[34]

$$V_{\mathrm{ex}}^{\mathrm{rods}} = \frac{\pi}{2} D L^2 = 2 \frac{L}{D} V_{\mathrm{rod}}, \quad \frac{L}{D} \gg 1, \tag{11}$$

where $V_{\mathrm{rod}} = \pi D^2 L/4$ is the volume of a (cylindrical) rod. The excluded volume scales linearly with the aspect ratio. The excluded volume between two spheres, on the other hand, is given by

$$V_{\mathrm{ex}}^{\mathrm{spheres}} = 8 V_{\mathrm{sphere}}, \tag{12}$$

where $V_{\mathrm{sphere}} = \pi (2a_H)^3/6$ is the volume of a sphere with diameter $2a_H$. Pair interactions for rods become important at volume fractions that are an order L/D less than for spheres. The combination $\phi L/D$ is the excluded volume fraction that also appears in the isotropic–nematic phase coexistence densities,[34] ϕ_I and ϕ_N, and the random closed packed density of rods,[35] ϕ_{RCP}, where the low-shear viscosity of a rod suspension diverges

$$\phi_I \frac{L}{D} = 3.29; \quad \phi_N \frac{L}{D} = 4.19; \quad \phi_{\mathrm{RCP}} \frac{L}{D} = 5.4. \tag{13}$$

We note that the low-shear viscosity $\eta_L(\phi)$ of suspensions of rods with variable aspect ratio L/D can also be rescaled by plotting η_L as a function of the rescaled volume fraction $\phi L/D$.[35]

An alternative geometrical interpretation of the shape effect is as follows: In order to occupy the same volume with particles, one needs much more rods than spheres, since $V_{\mathrm{rod}} \ll V_{\mathrm{sphere}}$ (provided that the rods are long and thin and $2a_H \cong L$):

$$\frac{n(\mathrm{rod})}{n(\mathrm{sphere})} = \frac{V_{\mathrm{sphere}}}{V_{\mathrm{rod}}} = \frac{2}{3} \frac{(2a_H)^3}{L D^2} \cong \frac{2}{3} \left(\frac{L}{D} \right)^2. \tag{14}$$

The number density of particles interacting with a given tracer sphere is thus a factor $(L/D)^2$ larger in case of rods than in case of spheres. If this is the dominant shape effect, plotting the mobility data as a function of particle number density should collapse the rod and sphere data. As seen in Fig. 5(b), plotting the two data sets versus *n* indeed results in practically identical concentration-dependencies.

Figures 5(a) and 5(b) suggest that the effect of the host particle shape on the rotational tracer dynamics can be explained by simple geometrical arguments. We believe that this issue merits future theoretical work. Additionally, it would be interesting to perform TPA measurements for tracer spheres in suspensions of rods with various aspect ratios L/D.

C. SED scaling

In Sec. III C 2 we address the applicability of Stokes–Einstein–Debye (SED) scaling of the rotational dynamics of the tracer spheres with the viscosity of the rod suspensions. Section III C 1 first presents the ionic strength and rod concentration dependence of the viscosity.

1. Low-shear viscosity of the host rod suspensions

Figure 6(a) shows the concentration dependence of the reduced low-shear-limiting viscosity $\eta_L(\phi)/\eta_0$ of the host rod suspensions at LiCl concentrations of 0, 1, 10, and 100

Downloaded 30 Mar 2011 to 130.37.129.78. Redistribution subject to AIP license or copyright; see http://jcp.aip.org/about/rights_and_permissions

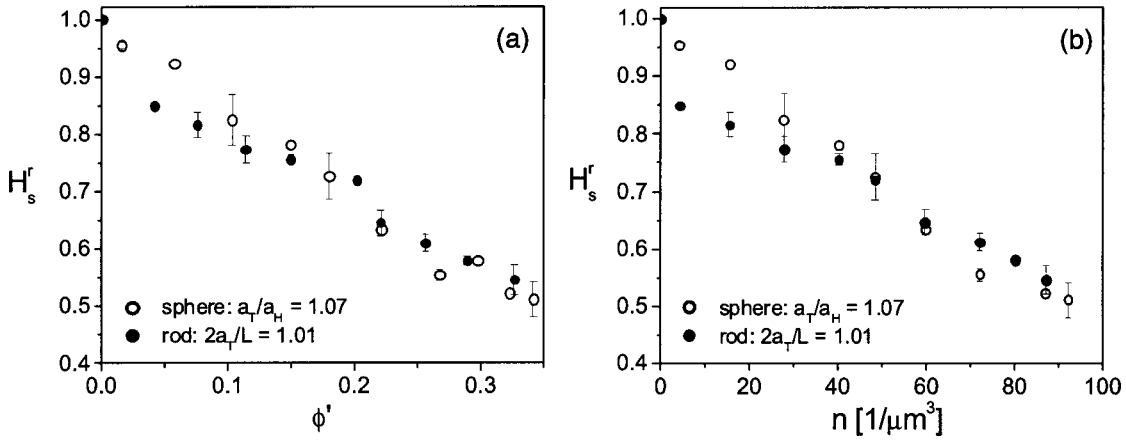

FIG. 5. Reduced short-time rotational diffusion coefficient $H_s^r(\phi)$ of charged μ30 tracer spheres in suspensions of host spheres and host rods, replotted as a function of the (a) rescaled volume fraction ϕ' (where $\phi'=\phi$ for the spheres and $\phi'=\phi\overline{L}/\overline{D}$ for the rods), and the (b) host particle number density n.

mM. At each LiCl concentration the viscosity increases as the rod concentration is raised due to hydrodynamic and direct interactions between the rods. Adding 1 mM LiCl to an initially salt-free dispersion of rods leads to a significant reduction of $\eta_L(\phi)$. Addition of 10 mM LiCl further reduces $\eta_L(\phi)$, but subsequent addition of 100 mM LiCl does not significantly alter $\eta_L(\phi)$. This rheological behavior suggests that double layer repulsions are long-ranged compared to the particle dimensions for LiCl concentrations below 10 mM. Above 10 mM, however, the double layers are compressed sufficiently to give a salt-independent viscosity, which is most likely equivalent to a hard-rod viscosity given the absence of significant dispersion forces.

Theoretical predictions of $\eta_L(\phi)/\eta_0$ for rod suspensions exist only for the case of infinite aspect ratio, monodisperse, hard rods. Recently, Dhont and Briels[20] showed that up to the isotropic–nematic phase transition, the viscosity is linear in ϕ

$$\eta_L(\phi)/\eta_0 = 1+[\eta]\phi, \tag{15}$$

with the intrinsic viscosity $[\eta]$ defined by the Onsager result[36]

$$[\eta]=\frac{8}{45}\frac{r^2}{\ln r}, \tag{16}$$

with $r=L/D$ the aspect ratio. The dotted line in Fig. 6(a) represents the theoretical prediction of Eq. (15) for monodisperse hard rods with aspect ratio $r=11.3$, using $[\eta]=9.3$. The solid line represents the theoretical prediction of Eq. (15), with $[\eta]$ corrected for the finite value of the aspect ratio using the theory of Kuhn and Kuhn[37] ($[\eta]\approx 20$). Both predictions significantly underestimate the actual viscosity. In addition, the experimentally observed ϕ-dependencies are nonlinear in contrast to Eq. (15). This discrepancy is most likely due to the finite length of the rods, which invalidates the assumptions made to derive Eq. (15). These assumptions involve the neglect of hydrodynamic interactions as well as third and higher-order virial coefficients in the virial expansion of the free energy.[20] HI cannot actually be neglected for short rods.[38] Since the precise form of the hydrodynamic interaction tensors for rods is unknown, explicit calculations of the viscosity of short rods are not available. HI are expected to lead to nonlinear contributions in ϕ to the zero-shear viscosity.[38,39] The third virial coefficient in the virial expansion of the free energy of hard rods cannot be neglected for $r\leqslant 50$.[40,41] It is unclear how this would affect the concentration dependence of the viscosity.

Figure 6(a) demonstrates that double layer repulsions increase the viscosity. The viscosity increase has two sources,

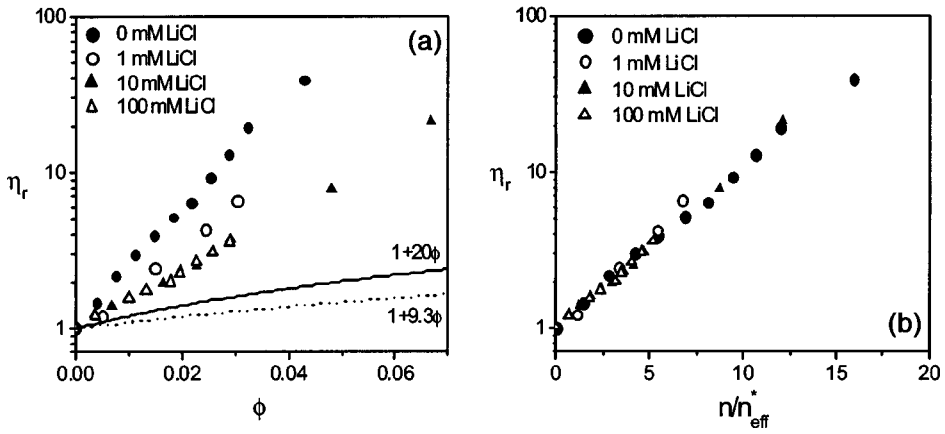

FIG. 6. (a) Low-shear-limiting viscosity $\eta_r=\eta_L/\eta_0$ of suspensions of host rods in DMF as a function of the rod volume fraction ϕ, for LiCl concentrations as indicated. The rod overlap volume fraction ϕ^* is around 0.008. The dotted and solid lines represent the theoretical predictions of Eq. (15) for monodisperse hard rods with aspect ratio $r=L/D=11.3$ without ($[\eta]=9.3$) and with ($[\eta]=20$) end-cap corrections, respectively. (b) Viscosity plotted as a function of the rescaled rod number density n/n^*_{eff} defined in Eq. (17), using $\alpha=3$.

Downloaded 30 Mar 2011 to 130.37.129.78. Redistribution subject to AIP license or copyright; see http://jcp.aip.org/about/rights_and_permissions

namely the primary electroviscous effect caused by shear-distortion of the double layers, which enhances $[\eta]$, and the secondary electroviscous effect, relating to direct interactions between double layers of different rods.[42] A calculation of the secondary electroviscous effect for rods is still lacking. For spheres this effect can be quite large, depending on the degree of screening.[42] In a recent study of the low-shear viscosity of aqueous dispersions of boehmite rods as a function of ionic strength[43] it was found that double-layer effects can be rescaled by normalizing the rod number density n by the effective minimum overlap concentration $n^*_{\mathrm{eff}}=(L+\alpha\kappa^{-1})^{-3}$ of rods with an effective length $L_{\mathrm{eff}}=L+\alpha\kappa^{-1}$. Here, α is a positive fit parameter, expected to be dependent on the rod charge. While uncharged rods start to interact when the average inter-rod separation is of order L, charged rods with extended double layers already have an interaction energy of order k_BT when the separation distance is L enlarged by several times κ^{-1}. The Debye screening length κ^{-1} is assumed to be independent of ϕ, which is reasonable for rod suspensions since $\phi \ll 1$. Figure 6(b) shows that the viscosity data for silica-boehmite rods in DMF also follow a single master curve after the scaling $\eta(\phi,\kappa^{-1})\rightarrow\eta(n/n^*_{\mathrm{eff}})$ with

$$n/n^*_{\mathrm{eff}}=\phi\frac{4}{\pi}\frac{\overline{L^2}}{\overline{D^2}}\left(1+\alpha\frac{\kappa^{-1}}{\overline{L}}\right)^3. \tag{17}$$

The best fit value $\alpha=3$ is similar to the value $\alpha=5$ reported for boehmite rods in water.[43] Note that the scaling approach neglects concentration effects on the Debye length (which are important when no LiCl is added) as well as polydispersity effects.

Similar excluded volume or effective hard rod arguments have been used by others to interpret translational[24] and rotational[44] dynamics of charged rods and the shift of phase coexistence densities[40,45,46] with ionic strength. It was proposed that the effective excluded volume of two charged rods is $B_2^{\mathrm{eff}}=L^2D^{\mathrm{eff}}\pi/4$, with D^{eff} an effective diameter according to $D^{\mathrm{eff}}=D+\alpha'\kappa^{-1}$.[24,40,45,46] The parameter α' was estimated from the distance where the electrostatic repulsion for two parallel rods is $1k_BT$ per rod, using expressions of Sparnaay[47]

$$\alpha\cong\ln\left[64\sqrt{\frac{\pi}{2}}cN_{\mathrm{av}}\tanh^2\left(\frac{e|\psi|}{4k_BT}\right)\sqrt{DL^2\kappa^{-3}}\right], \tag{18}$$

with c the molar salt concentration (mol/m^3), N_{av} the constant of Avogadro and Ψ the surface potential. Taking Ψ equal to the zeta potential, which is -24 mV for our rods in DMF in the presence of 10 mM LiCl ($\kappa^{-1}=2.26$ nm), we find $\alpha'=4.3$, close to our experimental finding of $\alpha=3$.

2. SED scaling

Figure 7 tests the applicability of SED scaling according to $H_s^r=\eta_0/\eta_L$, by plotting the product $H_s^r\eta_L/\eta_0$ as a function of rod volume fraction ϕ. SED scaling would imply $H_s^r\eta_L/\eta_0=1$. As seen, deviations from SED scaling at all ionic strengths are similar for the two smaller tracers ($a_T=67$ and 103 nm), while the largest tracer ($a_T=137$ nm) displays significantly smaller deviations. This is in agreement with the intuitive expectation that the accuracy of SED scaling should improve with increasing tracer–host size ratio: the inherently discontinuous nature of the colloidal host suspension should be less apparent to a larger tracer. For tracer–host sphere mixtures deviations from SED scaling were likewise found to decrease with increasing tracer–host particle size ratio.[16] Theoretical calculations on SED scaling for binary sphere mixtures were performed by Almog and Brenner,[48] who referred to the noncontinuum behavior in colloidal suspensions as a ''Knudsen-type'' slip-velocity size effect. For molecular-sized tracers performing rotational dif-

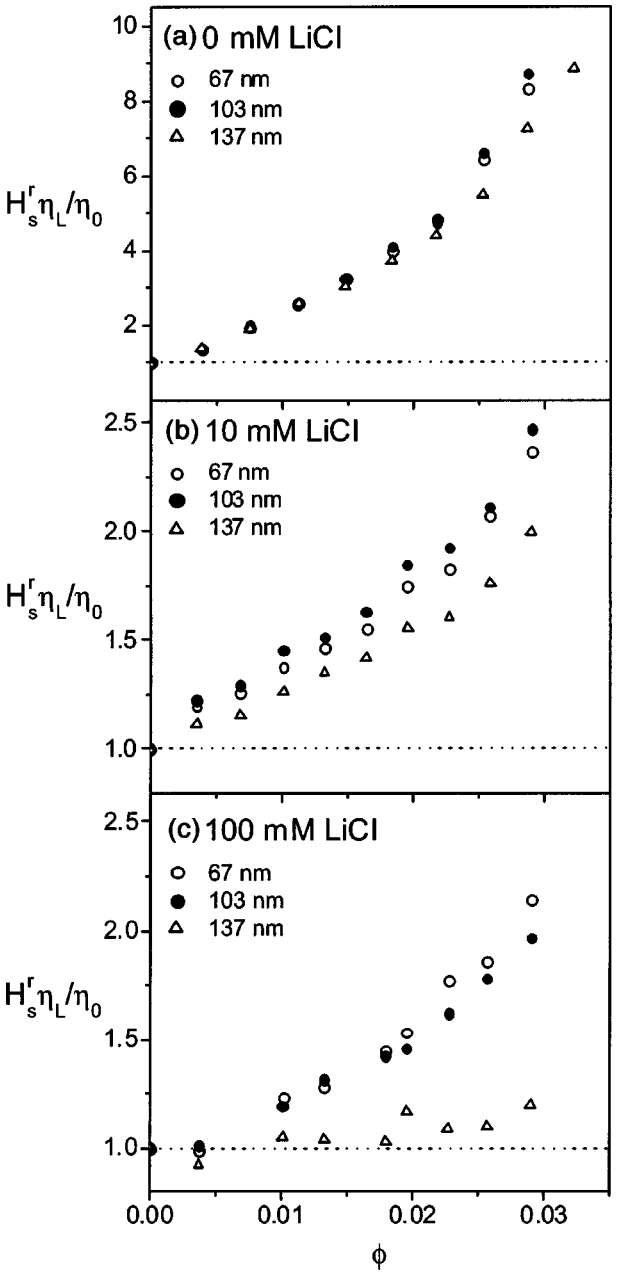

FIG. 7. Experimental test of SED scaling of the reduced tracer rotational diffusion coefficient H_s^r with the inverse reduced low-shear viscosity η_0/η_L of the host rod suspensions. Data are shown for LiCl concentrations of (a) 0, (b) 10, and (c) 100 mM. SED behavior implies $H_s^r\eta_L/\eta_0=1$ (dotted line). Note the different vertical scales of (b) and (c) compared to (a).

Downloaded 30 Mar 2011 to 130.37.129.78. Redistribution subject to AIP license or copyright; see http://jcp.aip.org/about/rights_and_permissions

fusion in simple solvents, deviations from SE(D) scaling are generally rationalized by assuming that partial slip of the fluid molecules occurs on the tracer surface

$$D_0^r = \frac{k_B T}{\nu_0^r (8\pi\eta_0 a_T^3)}. \tag{19}$$

The slip coefficient ν_0^r ranges from 1 (complete stick) to 0 (complete slip) depending on the size ratio between the solute and solvent molecules. In a completely analogous fashion deviations from SED behavior for rotational[15,16,48] and translational[25] diffusion of colloidal tracer spheres in colloidal sphere suspensions have been rationalized in terms of partial slip of the host particles. In the continuum limit $\lambda \gg 1$ the apparent slip coefficient is by definition equal to the stick value $\nu_s^r = 1$. Moving away from the continuum limit by lowering λ leads to values $\nu_s^r < 1$, reflecting the locally discontinuous nature of the neighborhood around a tracer sphere (which changes with ϕ). As a rodlike host particle approaches the surface of a tracer particle, its orientational degrees of freedom are reduced. This leads to an entropic repulsion between the tracer and the rod and the establishment of a depletion zone with reduced host concentration centered on each tracer. At the tracer surface the host particle concentration is on average zero, so the viscosity at this location equals the solvent viscosity η_0, leading to an apparent slip condition for the host particles. The tracer hydrodynamically interacts with the host particles over a layer of thickness Δ with a reduced viscosity and therefore probes a shear modulus that is smaller than the bulk modulus. With decreasing λ, the exclusion zone becomes wider until in the limit $\lambda \gg 1$ of a pointlike tracer (relative to a host sphere) one expects nearly perfect slip $\nu_s^r \approx 0$, since the tracer sees only solvent.[48] When the host particle concentration is increased the depletion layer thickness should remain virtually unchanged,[49] but the viscosity increment over the depletion zone increases. This explains the increase of the deviation from SED scaling with increasing host particle volume fraction.[11]

As seen in Fig. 7, the ionic strength of the host fluid strongly affects the applicability of SED scaling. At low ionic strength large deviations from SED scaling of up to a factor 10 are seen, whereas at high ionic strength the deviations are within a factor of 2. This behavior suggests that a continuous medium approach is already reasonable for fairly small tracer–host size ratios when double-layer repulsions are screened. However, long-ranged repulsions invalidate the continuum approach. This is in good qualitative agreement with experimental observations for binary mixtures of charged spheres.[13–16] The ionic strength dependence may be rationalized by observing that in charge-stabilized suspensions at low ionic strength the depletion zones surrounding the tracers are larger than in hard-particle suspensions, due to the strong long-range repulsions between the particles.[50] Equivalently, the failure of SED scaling at low ionic strength can be explained in terms of the slow effective structural relaxation time of the strongly interacting host particles. When the host particle dynamics is slow compared to the reorientation time of the tracer sphere, the tracer experiences a discontinuous environment with a locally reduced viscosity, i.e., $H_s^r \eta_L / \eta_0 > 1$. With increased screening of double-layer interactions, the structural relaxation time of the host particles is reduced, and the host suspension appears to the tracer more and more as a continuous medium. One indicator of the structural relaxation time of the host suspension is the low-shear viscosity, η_L. As seen in Fig. 6, η_L strongly rises with decreasing ionic strength, indicating slower dynamics.

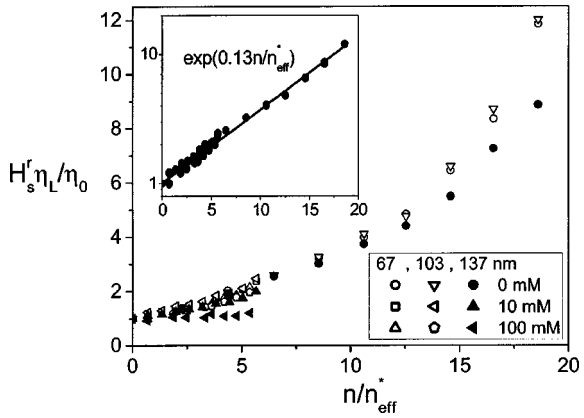

FIG. 8. SED product $H_s^r \eta_L / \eta_0$ as a function of the reduced number density n/n^*_{eff}, for the three different tracer spheres, each at three different LiCl concentrations. Inset shows semilogarithmic plot of all data for the two smallest tracers together with the best fit, $H_s^r \eta_L / \eta_0 = \exp(0.13 n/n^*_{\text{eff}})$.

Figure 8 shows that the dynamic rescaling procedure used in Fig. 6(b) to rescale the low-shear viscosities can also be applied with reasonable success to the SED products $H_s^r \eta_L / \eta_0$, at least for the two smallest tracers ($a_T = 67$ and 103 nm), choosing $\alpha = 4$. The data collapse onto a single exponential-like form according to $H_s^r \eta_L / \eta_0 \cong \exp(0.13 n/n^*_{\text{eff}})$, as shown in the inset. The scaling procedure is less accurate, however, for the largest tracer, with a radius $a_T = 137$ nm.

IV. CONCLUSIONS

We have measured the concentration dependence of the short-time rotational diffusion coefficient $H_s^r(\phi)$ of charged tracer spheres with radii of 67, 103, and 137 nm in suspensions of charged rigid rods as a function of the ionic strength, using TPA. The ionic strength dependence was qualitatively similar to that observed previously for tracer–host sphere mixtures. Reducing the Debye screening length κ^{-1} from 20 to 2.3 nm had no significant effect on the tracer mobility, but a further reduction of κ^{-1} to 0.96 nm led to a reduction of $H_s^r(\phi)$, due to stronger hydrodynamic coupling between the tracer and the rods. We suspect that tracer diffusion in rod suspensions is, like tracer diffusion in sphere suspensions, very sensitive to deviations from a hard-core potential, such as residual electrostatic repulsions and solvation effects. Theory or simulations are needed to confirm this idea.

We compared the results, in the high salt limit, with earlier TPA results for rotational dynamics of tracers in suspensions of host spheres with a diameter $2a_H \cong L$. The dependence of the tracer mobility on the host particle volume fraction is stronger for rods compared to spheres by a factor

Downloaded 30 Mar 2011 to 130.37.129.78. Redistribution subject to AIP license or copyright; see http://jcp.aip.org/about/rights_and_permissions

equal to the aspect ratio L/D. This suggests that the primary shape effect is the geometrical effect of the larger excluded volume of long and thin rods.

Finally we compared the tracer diffusion coefficients $H_s^r(\phi)$ with the low-shear viscosities η_L of the background host fluids and investigated the applicability of Stokes–Einstein–Debye (SED) scaling, $H_s^r \eta_L / \eta_0 = 1$. At low ionic strength ($\kappa^{-1} \approx 20$ nm) large deviations from SED scaling were observed for all three tracers, but with increasing ionic strength the relative deviation from SED scaling became less than a factor of 2 for the smallest tracers and close to 1 for the largest tracer. Double-layer effects can be rationalized in terms of an effective hard-rod model with the bare length L replaced by an effective length $L + 4\kappa^{-1}$. A more rigorous quantitative analysis of SED scaling would require experimental data and theoretical calculations for the infinite frequency (short-time) viscosity of suspensions of finite aspect ratio rods. We hope that this experimental study will stimulate theoretical and computer simulation work in order to have a firmer understanding of dynamics in rod–sphere mixtures.

In principle the experimental model system and the technique used in this work are ideally suited to study also the ''opposite case'' of rod rotation in sphere suspensions, which has received some previous experimental[51] and theoretical[52–55] attention. TPA experiments could be done on trace amounts of silica-boehmite rods with phosphorescently labeled silica shells[22] in suspensions of unlabeled silica spheres.

ACKNOWLEDGMENTS

The authors thank M. P. Lettinga, G. Nägele, and J. K. G. Dhont for many helpful discussions. This work was financially supported by The Netherlands Organization for Scientific Research (NWO/Stichting Chemische Wetenschappen).

[1] A. P. Philipse and A. M. Wierenga, Langmuir **14**, 49 (1998).
[2] A. M. Wierenga and A. P. Philipse, Colloids Surf., A **137**, 355 (1998).
[3] F. M. van der Kooij, E. S. Boek, and A. P. Philipse, J. Colloid Interface Sci. **235**, 344 (2001).
[4] A. G. Ogston, B. N. Preston, and J. D. Wells, Proc. R. Soc. London, Ser. A **333**, 297 (1973).
[5] R. I. Cukier, Macromolecules **17**, 252 (1984).
[6] A. R. Altenberger, M. Tirrell, and J. S. Dahler, J. Chem. Phys. **84**, 5122 (1996).
[7] D. S. Clague and R. J. Phillips, Phys. Fluids **8**, 1720 (1996).
[8] M. A. Tracey and R. Pecora, Macromolecules **25**, 337 (1992).
[9] M. R. Wattenberger, V. A. Bloomfield, Z. Bu, and P. S. Russo, Macromolecules **25**, 5263 (1992).
[10] M. A. Tracey, J. L. Garcia, and R. Pecora, Macromolecules **26**, 1862 (1993).
[11] D. Gold, C. Onyenemezu, and W. G. Miller, Macromolecules **29**, 5710 (1996).
[12] S. G. J. M. Kluijtmans, G. H. Koenderink, and A. P. Philipse, Phys. Rev. E **61**, 626 (2000).
[13] G. H. Koenderink and A. P. Philipse, Langmuir **16**, 5631 (2000).
[14] G. H. Koenderink, H. Zhang, M. P. Lettinga, G. Nägele, and A. P. Philipse, Phys. Rev. E **64**, 022401 (2001).
[15] G. H. Koenderink, M. P. Lettinga, and A. P. Philipse, J. Chem. Phys. **117**, 7751 (2002).
[16] G. H. Koenderink, H. Zhang, D. G. A. L. Aarts, M. P. Lettinga, A. P. Philipse, and G. Nägele, Faraday Discuss. **123**, 335 (2003).
[17] V. Degiorgio, R. Piazza, and R. B. Jones, Phys. Rev. E **52**, 2707 (1995).
[18] J. Kanetakis, A. Tolle, and H. Sillescu, Phys. Rev. E **55**, 3006 (1997).
[19] M. P. Lettinga, M. A. M. J. Van Zandvoort, C. M. van Kats, and A. P. Philipse, Langmuir **16**, 6156 (2000).
[20] J. K. G. Dhont and W. J. Briels, Colloids Surf., A **213**, 131 (2003).
[21] P. A. Buining, C. Pathmamanoharan, J. B. H. Jansen, and H. N. W. Lekkerkerker, J. Am. Chem. Soc. **74**, 1303 (1991).
[22] M. P. B. van Bruggen, Langmuir **14**, 2245 (1998).
[23] M. M. Tirado, J. Chem. Phys. **81**, 2047 (1984).
[24] M. P. B. van Bruggen, H. N. W. Lekkerkerker, and J. K. G. Dhont, Phys. Rev. E **56**, 4394 (1997).
[25] A. Imhof, A. Van Blaaderen, G. Maret, and J. G. K. Dhont, J. Chem. Phys. **100**, 2170 (1994).
[26] L. Helden, R. Roth, G. H. Koenderink, P. Leiderer, and C. Bechinger, Phys. Rev. Lett. **90**, 048301 (2003).
[27] J. R. Chipperfield, *Non-Aqueous Solvents* (Oxford University Press, Oxford, 1999).
[28] L. Helden, G. H. Koenderink, P. Leiderer, and C. Bechinger, (to be published).
[29] M. P. Lettinga, C. M. van Kats, and A. P. Philipse, Langmuir **16**, 6166 (2000).
[30] P. Debye, *Polar Molecules* (Dover, New York, 1929).
[31] M. P. Lettinga, H. Zuilhof, and M. A. M. J. van Zandvoort, Phys. Chem. Chem. Phys. **2**, 3697 (2000).
[32] M. Watzlawek and G. Nägele, Physica A **235**, 56 (1997).
[33] R. K. Iler, *The Chemistry of Silica* (Wiley, New York, 1979).
[34] L. Onsager, Ann. N.Y. Acad. Sci. **51**, 627 (1949).
[35] A. P. Philipse, Langmuir **12**, 1127 (1996).
[36] L. Onsager, Phys. Rev. **40**, 1028 (1932).
[37] W. Kuhn and H. Kuhn, Helv. Chim. Acta **28**, 97 (1945).
[38] E. S. G. Shaqfeh and G. H. Fredrickson, Phys. Fluids A **2**, 7 (1990).
[39] I. L. Claeys and J. F. Brady, J. Fluid Mech. **251**, 443 (1993).
[40] T. Odijk, Macromolecules **19**, 2313 (1986).
[41] H. N. W. Lekkerkerker and G. J. Vroege, Philos. Trans. R. Soc. London, Ser. A **344**, 419 (1993).
[42] W. B. Russel, J. Fluid Mech. **85**, 209 (1978).
[43] A. M. Wierenga and A. P. Philipse, Langmuir **13**, 4574 (1997).
[44] A. M. Wierenga, A. P. Philipse, and E. M. Reitsma, Langmuir **13**, 6947 (1997).
[45] A. Stroobants, H. N. W. Lekkerkerker, and T. Odijk, Macromolecules **19**, 2232 (1986).
[46] G. J. Vroege and H. N. W. Lekkerkerker, Rep. Prog. Phys. **55**, 1241 (1992).
[47] M. J. Sparnaay, Recueil **78**, 681 (1959).
[48] Y. Almog and H. Brenner, Phys. Fluids **10**, 750 (1998).
[49] L. Auvray, J. Physique **42**, 79 (1981).
[50] D. A. Hoagland, Macromolecules **23**, 2781 (1990).
[51] J. K. Phalakornkul, A. P. Gast, and R. Pecora, J. Chem. Phys. **112**, 6487 (2000).
[52] R. Pecora and J. M. Deutch, J. Chem. Phys. **83**, 4823 (1985).
[53] K. Raghavan, Mol. Phys. **84**, 345 (1995).
[54] S. Ravichandran and B. Bagchi, J. Chem. Phys. **111**, 7505 (1999).
[55] F. D. Guevara-Rodriguez and M. Medina-Noyola, Phys. Rev. E **61**, 6368 (2000).

Downloaded 30 Mar 2011 to 130.37.129.78. Redistribution subject to AIP license or copyright; see http://jcp.aip.org/about/rights_and_permissions